Field Oriented Control of Multiphase Drives with Passive Fault-Tolerance

I. González Prieto, M.J. Duran, P. Entrambasaguas, M. Bermudez

***Abstract*– Multiphase machines provide continuous operation of the drive with no additional hardware in the event of one or more open-phase faults. This fault-tolerant capability is highly appreciated by industry for security and economic reasons. However, the steady-state post-fault operation has only been feasible in previous works after the fault localization and control reconfiguration. Even though this is done at the software stage, the obligation to identify the faulty phases and store the modifications for every fault scenario adds further complexity. This work reveals that this software reconfiguration can be avoided if the field-oriented control (FOC) strategy is designed to satisfactorily handle pre- and post-fault situations. Experimental results confirm the capability to obtain suitable post-fault operation without fault localization and control reconfiguration, thus achieving a passive/natural fault tolerance.**

Index Terms*– Fault tolerance, field-oriented control, induction motors, multiphase drives.

I. Introduction

Fault tolerance of electric drives has been intensively studied because the reliability obtained from the continuous operation brings benefits in terms of economy and security. While fault tolerance is mandatory in safety-critical applications (e.g. electric vehicles or aircraft), it brings economic benefits in applications where the corrective maintenance might become temporarily unfeasible (e.g. offshore wind energy systems) [1-6].

Standard three-phase electric machines are inherently non-tolerant to open-phase faults (OPF) because losing one phase makes the machine single-phase. Torque ripple and vibrations are then inevitable, and the steady-state performance of the drive is compromised. Consequently, the only manner to add further reliability against OPF is including some additional hardware [7]. Incipient faults result in high resistance values of the faulty phase, and the resulting dissymmetry can be compensated with a proper design of the controllers [8]. This work focuses however on OPF, which are the most common type of faults analyzed in the field of multiphase drives.

Opposite to standard three-phase systems, multiphase drives (more than three phases) do not need any additional hardware to provide a satisfactory post-fault operation, this being one of their most remarkable features [9-14].

Manuscript received August 2, 2018; revised March 17, 2019; revised May 30, 2019; revised August 5, 2019; accepted September 9, 2019.

This research was funded by the Spanish Government under the Plan Estatal 2017-2020 with the reference RTI2018-096151-B-I00.

I. Gonzalez-Prieto M.J. Duran and P. G. Entrambasaguas are with the Department of Electrical Engineering at the University of Malaga, Spain, e-mail: ignaciogp87@gmail.com, mjduran@uma.es and paulaentrambasaguas@gmail.com.

M. Bermudez is with the Department of Electrical Engineering at the University of Huelva, Spain, e-mail: mariobermg@gmail.com.

Nevertheless, a satisfactory post-fault operation can only be achieved if the closed-loop control is previously informed about the specific fault scenario and it is conveniently reconfigured.

Even though there is no need for extra hardware, this fault tolerance is achieved at the expense of additional software complexity. First of all, it is necessary to detect the fault in order to appropriately derate the drive [15-16]. Nevertheless, the fault detection is not sufficient because the control stage needs information about the phase(s) under OPF. Hence, it becomes mandatory to localize the fault(s) and determine the fault scenario in order to properly reconfigure the regulation strategy [15-16]. In a n-phase electric drive the identification of the faulty phase requires at least n fault indices, so the complexity of the localization stage grows with the number of phases. Although, it does not imply an excessive computational burden, avoiding the identification process provides some further simplicity.

Unfortunately, the reconfiguration of the control scheme is different for each fault scenario and the number of fault scenarios in a n-phase machine with single star-connected neutral is equal to n for single-phase faults and $(n-1)\cdot n/2$ for double-phase fault. Consequently, it is necessary to store as many post-fault control settings as possible fault scenarios. The approach for the reconfiguration is quite different depending on the control strategy. In direct torque control (DTC) it is necessary to define different look-up tables for each fault scenario [17], whereas in model predictive control (MPC) it is necessary to define new Clarke transformations, references and cost functions [18]. Finally, field-oriented control (FOC) needs to modify the references of the secondary currents (typically termed x-y currents in literature [1-2]) and switch from proportional-integer (PI) to proportional-resonant (PR) controllers in order to track both positive and negative sequence components [9, 17-19]. Since the new current references depend on the fault scenario, it is necessary to store off-line all post-fault possible references and choose the correct one immediately after the fault has been localized. A comparison of post-fault FOC and MPC strategies with the aforementioned reconfigurations can be found in [17-18].

The previously described fault localization and control reconfiguration provides well-proved fault tolerant capability [9-21] and it can be currently considered as the standard procedure to achieve a satisfactory post-fault operation. However, it is achieved at the expense of a software reconfiguration for a rather extensive range of possibilities. There is, however, an alternative to the reconfiguration approach: to analyze the reasons why pre-fault control strategies fail and to devise a universal control scheme that simultaneously brings a good regulation before

and after the OPF occurrence. This capability to achieve a satisfactory post-fault performance (in the same range as in reconfigured fault-tolerant FOC) without the need to make any modification in the control strategy will be referred in what follows as *passive/natural fault tolerance*.

This work follows this path and presents the following contributions:

C1) The two main causes of FOC inaccuracy after the OPF occurrence are discussed together with an analysis of the impact of each one on the drive performance.

C2) It is verified that keeping the x-y current control in open-loop mode results in a satisfactory post-fault performance.

C3) Different approaches for the deactivation of the x-y current control loops in post-fault operation are proposed and it is finally confirmed that a natural fault tolerance is feasible.

The analysis in C1 concludes that the main problem of pre-fault strategies is that different controllers are seeking incompatible goals after the OPF occurrence. Hence, it is verified in C2 that the deactivation of the x-y closed-loop control provides a natural post-fault operation. C3 finally presents different manners to obtain a passive fault-tolerant capability with an open-loop x-y current control. The suggested approach fully maintains the pre-fault performance and, at the same time, provides *i)* a remarkable simplification to design software-less fault-tolerant electric drives for industrial applications and *ii)* an enhanced robustness since the post-fault performance is not affected by fault detection delays or errors.

II. FIELD ORIENTED CONTROL OF SIX-PHASE INDUCTION MOTOR DRIVES

The general principles of field-oriented control electric drives date back to the early 1970s [22], although it was not until the early 1980s that it was implemented in reality thanks to more powerful digital signal processors (DSPs) and advanced power electronics.

A. FOC in pre-fault situation for multiphase drives

The extension of FOC to multiphase drives has also been accomplished and intensively applied since the beginning of the 21st century [1,4-5]. When the induction machine is assumed to have distributed windings and spatial harmonics are neglected, the extension of FOC is rather simple since the model in the d-q subspace presents no differences compared to the three-phase case. Although it is possible to adopt a double-dq approach for six-phase drives by defining one pair of d-q currents for each three-phase set [23-25], it provides a better insight and it is more widely accepted the use of the vector space decomposition (VSD) that results from the following Clarke transformation [4]:

$$[T]=\frac{1}{\sqrt{3}}\begin{bmatrix}1 & -1/2 & -1/2 & \sqrt{3}/2 & -\sqrt{3}/2 & 0\\ 0 & \sqrt{3}/2 & -\sqrt{3}/2 & 1/2 & 1/2 & -1\\ 1 & -1/2 & -1/2 & -\sqrt{3}/2 & \sqrt{3}/2 & 0\\ 0 & -\sqrt{3}/2 & \sqrt{3}/2 & 1/2 & 1/2 & -1\\ 1 & 1 & 1 & 0 & 0 & 0\\ 0 & 0 & 0 & 1 & 1 & 1\end{bmatrix} \quad (1)$$

$$\left[i_\alpha, i_\beta, i_x, i_y, i_{0+}, i_{0-}\right]^T = [T]\cdot[i_{a1}, i_{b1}, i_{c1}, i_{a2}, i_{b2}, i_{c2}]^T$$

If the machine is arranged with two isolated neutrals, zero-sequence currents (i_{0+}, i_{0-}) are null and consequently can be omitted from the analysis.

The control structure shown in Fig. 1 follows the classical nested structure with an outer PI controller for the speed regulation and inner PI controllers for the regulation of stator currents in VSD frame. Assuming two isolated neutrals, it is only necessary to measure four phase currents (i_{a1}, i_{b1}, i_{a2} and i_{b2}), which are then converted into VSD variables using the Clarke transformation from (1). The α-β currents of the fundamental plane are transformed to synchronous reference frame using the Park rotational transformation:

$$[D]=\begin{bmatrix}\cos\theta_s & \sin\theta_s\\ -\sin\theta_s & \cos\theta_s\end{bmatrix} \quad (2)$$

$$\left[i_d, i_q\right]^T = [D]\cdot\left[i_\alpha, i_\beta\right]^T \qquad \left[i_{x'}, i_{y'}\right]^T = [D]\cdot\left[i_x, i_y\right]^T$$

where the rotor flux reference frame is indirectly obtained from the rotor parameters and the measured currents in order to make the estimation independent from the current tracking performance [26-27]:

$$\theta_s = \int(\omega_r + \omega_{sl})\cdot dt = \int\left(\omega_r + \frac{R_r\cdot i_q}{L_r\cdot i_d}\right)\cdot dt \quad (3)$$

As in three-phase FOC, the d-current is then controlled to achieve rated flux in the base-speed region and the q-current is regulated to provide the necessary torque reference from the outer speed loop. The x-y current regulation can be simply done in open-loop mode by setting null voltages in this subspace (i.e. $v_{xy}^*=0$). Although in principle null x-y voltages should theoretically lead to null x-y currents, some inevitable phenomena such as asymmetries in the machine, in the voltage supply, spatial harmonics in the airgap or non-null inverter dead-time can induce some undesirable circulating currents that diminish the drive efficiency [23-25]. For this reason, the indirect rotor FOC version with an additional pair of PI controllers for the x-y subspace has been the most popular choice in recent times [1,4,9] (see Fig. 1a) to compensate the aforementioned asymmetries. The output of the x-y current regulators provides the x-y voltage references.

It is worth noting that d-q and x-y subspaces are orthogonal, and this implies that they can be independently regulated [4]. Consequently, the current references in both planes can be tracked with no disturbance/interaction of the d-q and x-y controllers (Fig. 2a).

B. FOC in post-fault situation for multiphase drives

After the satisfactory extension of FOC to multiphase drives in normal operation, the next challenge was to identify the necessary modifications in the control scheme to obtain a satisfactory post-fault operation. One mandatory action after the OPF is the fault detection and the reduction of the torque limit according to a predefined derating [2,11]. Nevertheless, the ripple-free post-fault operation requires two more steps: the fault localization and the reconfiguration of the control scheme.

Let us consider as an example the case when double OPF occur in phases a_1 and c_2. In this case the current cannot flow anymore through the faulty phases and this imposes the following physical restrictions from (1):

$$\begin{aligned} i_x &= -i_\alpha \\ i_y &= -i_\beta \end{aligned} \quad (4)$$

It is then necessary to identify that a_1 and c_2 are the faulty phases, and this requires the use of multiple fault indices [15-16]. Once the faults have been successfully localized, the

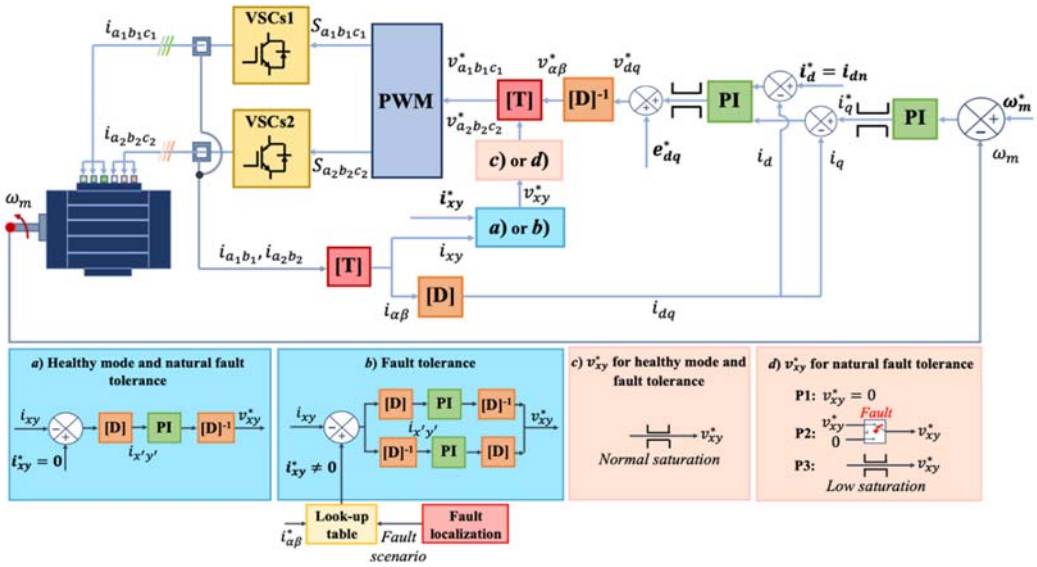

Fig. 1. Indirect rotor field-oriented control (IRFOC) of six-phase induction motor drives for: *i)* healthy operation (selecting a and c), *ii)* fault-tolerant operation with reconfiguration (selecting b and c) and *iii)* passive fault-tolerant operation (selecting a and d).

information from (4) is provided to the control and the current references are changed accordingly:

$$i_x^* = -i_\alpha^* \qquad i_y^* = -i_\beta^* \tag{5}$$

Although the α-β and x-y planes are no longer independent, the α-β and x-y controllers work together for a compatible aim thanks to the reconfiguration of the reference currents from (5) (see Fig. 2b). It is found however that the post-fault x-y current references are not constant in general, and it is then necessary to switch from PI to proportional-resonant (PR) controllers, which are typically implemented using two PI controllers in synchronous and anti-synchronous reference frames [9] (see Fig. 1b). The regulation of α-β currents remains the same and it is typically done in synchronous reference frame in order to generate the same rotating flux as in pre-fault condition [18]. As a summary, the main changes in the control scheme are the modifications of the current references and the use of PR controllers after the OPF occurrence.

III. Pre- fault Control Scheme Design to Achieve Passive Fault Tolerance

Even though the mainstream procedure for post-fault operation is the reconfiguration of the FOC scheme [11,17-19], it is possible to tackle the problem from a different perspective. Instead of determining the control modifications that need to be carried out after the fault occurrence, an alternative approach is to take preventive actions in the design of the pre-fault FOC strategy in order to achieve a natural fault tolerance. For this purpose, this section firstly analyses the problems of the pre-fault FOC strategy after the OPF occurrence (III.A), and then proposes a control strategy that achieves a satisfactory post-fault performance without fault localization and control reconfiguration (III.B).

A. Problems of pre-fault control strategies in faulty mode

The first problem that can be found after the OPF is the erroneous localization of the voltage vectors. Since the control strategy has not been informed about the OPF occurrence, the PWM stage still believes that the faulty phase is contributing to the output voltage generation. However, the switching state of the faulty VSC leg is irrelevant in OPF situation because the phase of the machine has been disconnected from the VSC leg. Fig. 3 shows the difference between the healthy (green circles) and faulty (red diamonds) voltage vectors when an open-phase fault occurs in phase a_1. Hence, from a qualitative point of view, Fig. 3 allows to know the error in the localization of the voltage vectors when pre-fault control strategies are employed in post-fault situation. This error appears due to the variation in the voltage generation produced by the fault. Although the shifting of the voltage vectors inevitably implies some inaccuracy in the control action, the closed-loop nature of the FOC can compensate this error, eventually driving the machine to the correct operating point. This statement will be confirmed later on with the experimental results detailed in section V.

The second problem comes from a different source and it is related to the conflict of controllers after the OPF. While FOC maintains the same number of controllers, the OPF diminishes the number of variables that can be controlled. Although it is clear from (4) that α-β and x-y currents are not independent anymore in faulty situation, FOC still maintains an independent action of the α-β and x-y PI controllers. If the target of the x-y controllers is still to keep the x-y currents around zero value ($i_{xy}^* = 0$) and the target of the α-β controllers is to track the flux and torque ($i_{\alpha\beta}^* \neq 0$), a conflict between both controllers becomes inevitable. The final value of α-β and x-y currents will be somewhere in the middle between the two incompatible objectives for $i_{\alpha\beta}^*$ and i_{xy}^* (Fig. 2b). This leads to some disturbance in the α-β plane that eventually leads to a poor post-fault performance.

Further delving into the conflict of the controllers, it can be deduced from (4) after a synchronous rotational transformation from (2) that a positive value of the q-current produces a negative y' current [10]. Consequently, the y' PI controller needs to apply a positive y' reference voltage to obtain a null value of the y' current. However, this y' PI controller action produces the q PI controller reaction, whose objective is to reach a non-null value of the q-current. For this reason, this conflict can be defined as an action-reaction problem that is inherently unstable. The parameters of the PI controllers will define the dynamics of the action-reaction process, but regardless of how slow/quick the

transient is, the conflict finishes when one of these controllers reaches its saturation voltage threshold. From the point of view of the machine control, there are two possible final scenarios of this action-reaction process:

S1) d-q PI controllers win the conflict: The d-q voltage does not reach the saturation threshold and therefore the tracking of the reference speed is suitable

S2) x'-y' PI controllers win the conflict: The d-q voltage reaches the saturation threshold and consequently the speed drops because the flux/torque are out of control.

B. Design of a pre-fault control strategy with a passive fault tolerance

Based on the previous analysis, the main cause for the flux/torque disturbance after the OPF is the conflict of the PI controllers used in FOC. It follows that deactivating the x-y current control after the fault occurrence should allow a ripple-free post-fault performance. While the open-loop x-y current control is inherently achieved with the use of virtual vectors in MPC [28], three possibilities are suggested for FOC in this work (Fig. 1d):

P1) Eliminate the closed-loop x-y current control and set $v_{xy}^{*}=0$.

P2) Maintain the closed-loop x-y current in healthy condition and switch to P1) after the OPF.

P3) Maintain the closed-loop x-y current control setting a low saturation threshold for v_{xy}^{*}.

The strategies P1, P2 and P3 can be mathematically expressed as:

$$\begin{aligned} P1 \rightarrow \quad & v_{xy}^{*}=0 && \forall t \\ P2 \rightarrow \quad & v_{xy}^{*}=P(e_{xy})+I\left(\int e_{xy}\right) && t\le t_f \\ & v_{xy}^{*}=0 && t>t_f \\ P3 \rightarrow \quad & v_{xy}^{*}=P(e_{xy})+I\left(\int e_{xy}\right) && [v_{xy}]\le v_{x'y'}^{max} \\ & v_{xy}^{*}=T_h && [v_{xy}]> v_{x'y'}^{max} \end{aligned} \tag{6}$$

where t_f if the instant when the OPF occurs, e_{xy} is the x-y current error that serves as an input for the x-y PI controller, and $v_{x'y'}^{max}$ is the threshold for the saturation of the x-y voltages (see Fig. 1d). As other fault-tolerant control approaches proposed in literature, strategies P1, P2 and P3 assume that the spatial harmonics of the machine can be neglected and the x-y currents are regulated to zero in healthy operation for the sake of efficiency.

Strategy P1 is well-known from the old days of multiphase FOC [23,29], but it has never been tested under OPF. Since the x-y control is performed in open-loop all the time, it provides a natural fault-tolerance. In spite of the simplicity, it is not a preferred choice because it is known that the open-loop x-y control in healthy condition is sensitive to asymmetries/ imperfections. It follows that strategy P1 is optimal from the fault-tolerant point of view, but it can spoil efficiency in healthy state due to the appearance of non-null x-y currents.

Strategy P2 solves the deficiencies of P1 in pre-fault situation because it keeps the closed-loop control in healthy state and only switches to the open-loop mode (setting $v_{xy}^{*}=0$) at $t=t_f$. Nevertheless, it does not bring a natural fault tolerance. Although the modifications in the control scheme are much simpler than those in standard post-fault strategies [9-19], the ripple-free operation still depends on the fault detection and requires some reconfiguration (i.e. deactivation of the x-y current loops).

Strategy P3 has the same pre-fault performance as P2 and provides the passive fault tolerance of P1. The main idea is to maintain the closed-loop x-y current control in healthy condition, forcing the drive to operate in scenario S1 after the OPF. By setting a sufficiently low value of the x-y voltage saturation threshold ($v_{x'y'}^{max}$), the escalation of the reference voltages reaches first the x-y plane and annuls the effect of the x-y PI controllers. In other words, the action-reaction process described in III.A results in the automatic deactivation of the x-y current control. Opposite to P2, the activation of the open-loop x-y control is achieved naturally, not forced by a switch. Hence, the control itself skips scenario S2 and enters into scenario S1, thus deactivating the closed-loop x-y control with no further action required. Hence, strategy P3 is immune to errors or delays in the fault detection process.

The selection of the threshold $v_{x'y'}^{max}$ in strategy P3 should be done on the basis of allowing the standard FOC operation in healthy condition and quickly deactivating the x-y current control after the OPF occurrence. For this purpose, the value of $v_{x'y'}^{max}$ must be set above the x-y voltage ripple in healthy state. If $v_{x'y'}^{max}$ is set much above the x-y voltage ripple, the deactivation of the x-y current controllers will be slightly slower, whereas very low values of $v_{x'y'}^{max}$ will deactivate the x-y current controllers even in healthy operation, eventually becoming strategy P1.

It must be highlighted that regardless of the strategy (P1, P2 or P3), the fault-tolerant operation requires a mandatory derating in order to keep the drive safe [11]. This procedure is exactly the same as in standard fault-tolerant strategies with control reconfiguration, and it can be simply implemented with a saturation of the q-current (see Fig. 1). The limits for the derating can be obtained from [11] taking into account that the drive follows a minimum copper loss post-fault operation [11,18]. The fault detection stage is necessary for the drive derating, but its delays or errors will not have an impact on the post-fault control performance. Consequently, a smooth transition from healthy to faulty states is expected.

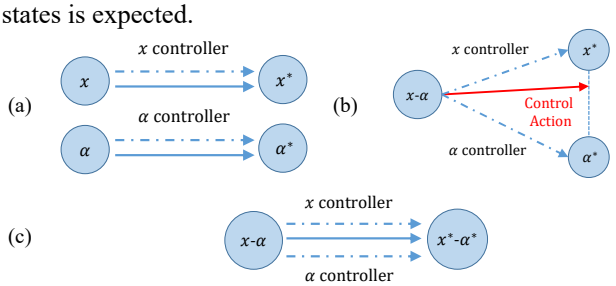

Fig. 2. Scheme of the control action: (a) Pre-fault situation, (b) post-fault situation without reconfiguration and (c) post-fault situation with reconfiguration.

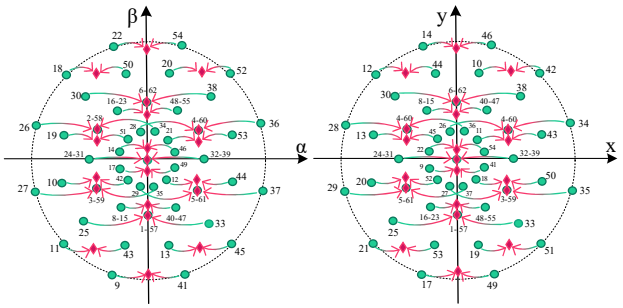

Fig. 3. Shifting of the voltage vectors when transiting from healthy (green circles) to faulty operation (red diamonds).

As a summary, the passive fault-tolerant strategy proposed in this work provides the following benefits compared to those approaches that require control reconfiguration:

- Simplicity: there are no changes at all in the control scheme. The lack of reconfiguration avoids the need to store off-line multiple post-fault control reconfiguration settings for each possible fault scenario, this resulting in a significant reduction of the control complexity.
- Robustness: the satisfactory post-fault operation is guaranteed regardless of the fault detection delays/errors. This property ensures a proper post-fault speed regulation and a smooth transient after the fault occurrence.

IV. Experimental Results

A. Experimental rig

The employed test bench is depicted in Fig. 4. An asymmetrical six-phase IM is supplied with conventional two-level three-phase VSCs (Semikron SKS22F modules). The parameters of the custom-built six-phase IM have been obtained using ac-time domain and stand-still with inverter supply tests [30-31]. These two standard estimation techniques have been employed in order to minimize the disturbances in the control due to a wrong estimation of the parameters. Table I shows the six-phase IM parameters.

A single dc power supplies the VSCs and the control actions are performed by a digital signal processor (TMS320F28335 from Texas Instruments, TI). The current and speed measurements are obtained using four hall-effect sensors (LEM LAH 25-NP) and a digital encoder (GHM510296R/2500), respectively. The six-phase IM is loaded coupling its shaft to a dc machine. The armature of the dc machine is connected to a variable passive R load that dissipates the power and the load torque is consequently speed-dependent.

On the other hand, the open-phase faults have been provoked using a controllable relay board implemented between the inverter and the machine connecting board. For this purpose, one free GPIO of the TMS320F28335 is used to active the relay. Hence the machine terminals are fully disconnected from the VSC and consequently the current cannot flow through the diodes.

B. Results

Test 1 is firstly designed to verify the contribution C2 of this manuscript, i.e. to confirm the satisfactory post-fault performance that can be obtained when the x-y current control is performed in open-loop mode (strategy P1 formerly described). Moreover, this test shows the influence of the x-y current controllers' parameters in the transition from pre- to post-fault situation. For that purpose, three different tuning for the x-y currents controllers have been analyzed: high-gain x-y PI controllers (left column of Fig. 5), low-gain x-y PI controllers (middle column of Fig. 5) and open-loop x-y current control (right column of Fig. 5). The parameter values of the x-y current controllers are included in table II. It is worth noting that there are tuning procedures based on measurements from the control [32]. However, since the main focus of this work is to demonstrate the natural fault-tolerant capability of FOC with minor changes, the tuning of PI controllers has been performed on an empirical basis using a trial and error procedure.

In test 1 the machine is driven at 500 rpm with d-current reference of 1.1 A and load torque of 3 Nm. At time t=5s two simultaneous OPF in phases a_1 and c_2 are provoked. According to [9], this fault scenario results in a reduction of 42% of the α-β current amplitude, but the rated currents from table I are not exceeded and consequently the drive can maintain the pre-fault torque and speed references. The currents cannot obviously flow through the damaged phases (see Figs. 5f and 5g) and, therefore, the two restrictions from (4) appear after the fault occurrence (see Fig. 5c). Since the control strategy is not reconfigured in test 1, the current controllers have now incompatible objectives ($i^*_{\alpha\beta} \neq 0$ whereas $i^*_{xy} = 0$) and there is a conflict of interest between α-β and x-y controllers. No matter if the x-y controllers are more or less aggressive (left and middle columns in Fig. 5, respectively), the closed-loop control eventually enters scenario S2 and the machine speed drops (Fig. 5a). After the fault occurrence, the conflict of controllers provokes an action reaction process that results in an escalation of the voltage references (Fig. 5e and 5f). This eventually saturates the q-voltage (Fig. 5e), and in turn the q-current (Fig. 5b). Since the q-current governs the electromechanical energy conversion process, after its saturation the system enters scenario S2 and loses the torque control. As expected, an aggressive x-y PI controller accelerates the saturation of the q-reference voltage (Fig. 5e, left plot) and therefore provokes an instantaneous speed drop. When the x-y PI controller is more relaxed, the q-voltage rises in a ramp-wise manner and the saturation is reached with some delay (Fig. 5e, middle plot). However, the PI parameters setting determines the dynamics of the post-fault transient but cannot avoid in any case the speed drop (Fig. 5a, left and middle plots).

The situation is completely different when the x-y current control is done in open-loop mode (Fig. 5, right plots). In this case the x'-y' voltage references are set to zero (Fig. 5f, right plots), this being in correspondence with strategy P1. In this case the speed is correctly maintained at 500 rpm (Fig. 5a, right plot) and the d-q currents are mostly similar before and after the fault occurrence (Fig. 5b, right plot). Even though the control is exactly the same during the whole test, the system presents a satisfactory ripple-free post-fault behavior with a similar performance as in the case when

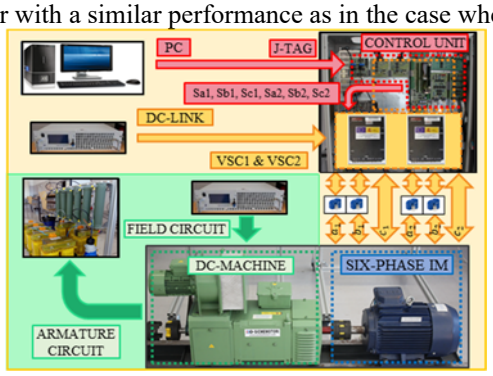

Fig.4. Test bench.

TABLE I
INDUCTION MOTOR PARAMETERS

R_s (Ω)	14.2
R_r (Ω)	2
L_m (mH)	420
L_{ls} (mH)	1.5
L_{lr} (mH)	55
T_{rated} $(N \cdot m)$	10.72
$\omega_{rated}(rpm)$	1000
$\lvert i_{phase}\rvert(A)$	3

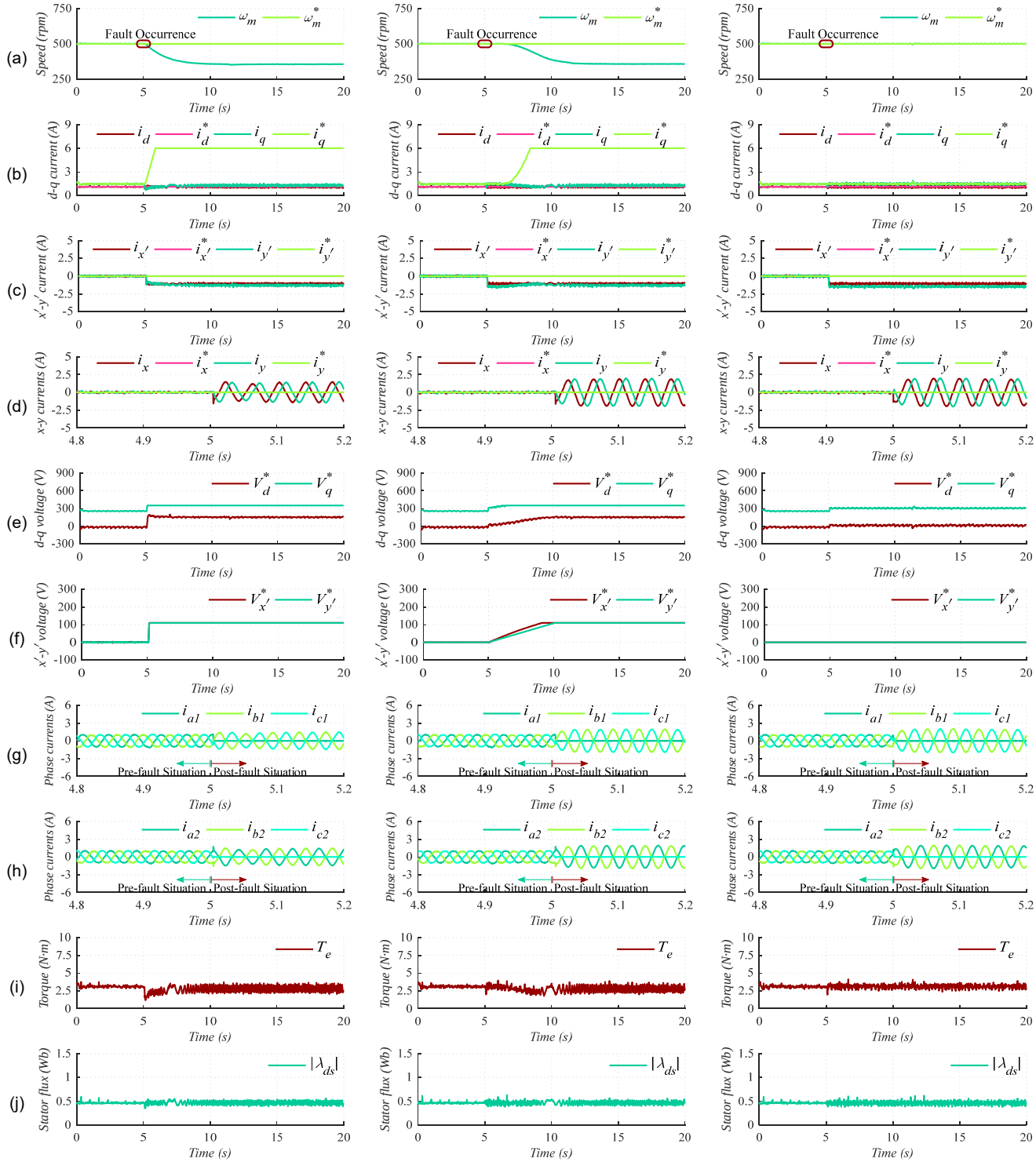

Fig. 5. Transition from pre- to post-fault situations for IRFOC with high-gain x-y PI controllers (left column), low-gain x-y PI controllers (middle column) and open-loop x-y current control (right column). From top to bottom: (a) Motor speed, (b) d-q currents, (c) x'-y' currents, (d) x-y currents, (e) d-q voltages, (f) x'-y' voltages, (g) $a_1b_1c_1$ phase currents, (h) $a_2b_2c_2$ phase currents, (i) electromagnetic torque and (j) stator flux.

TABLE II

PARAMETER VALUES OF THE X-Y CURRENT CONTROLLERS

Controller	K_P	K_I
High-gain x-y PI controllers	22.5	90
Low-gain x-y PI controllers	2.5	9

reconfigured fault-tolerant strategies are used [11]. It can be observed that the x-y currents cannot track the null references after the fault occurrence (Fig. 5d, right plots) because of the physical restrictions from (4). However, this tracking error does not provoke an escalation of the x'-y' voltages and the action-reaction process between α-β controllers is not triggered. The d-q voltage references are only slightly increased (Fig. 5e, right plot) in order to counteract the action of the x-y plane, but the escalation of the voltage references is not present anymore. Consequently, the system finds a stable operating point without exceeding any threshold for the voltage saturation. This implies that the system is operating in scenario S1 after the OPF and the performance of the speed tracking is satisfactory both in pre- and post-fault situations. Phase currents have the typical waveform that is obtained when the post-fault regulation is done with a reconfiguration of the control stage [2] (Figs. 5g and 5h, right plots), hence confirming that natural and reconfigured approaches provide a similar performance. Finally, Figs. 5i and 5j depict the theoretically estimated electromagnetic torque and stator flux in the transition from

pre- to post-fault situations. The resulting post-fault torque ripple when the control is not reconfigured and the x-y currents are regulated in open-loop mode (Fig. 5i, right plot) is kept in the same range as in conventional (i.e. reconfigured) fault-tolerant FOC [17]. When closed-loop x-y currents control exists (Fig. 5i, left and middle plots) the average value of the torque is slightly decreased after the OPF (from 3.1 to 2.6 Nm) and the ripple is increased. The post-fault ripple is kept relatively low because of the symmetry in the fault scenario of test 1 (phases a_1 and c_2 are spatially shifted by 90°). Since the speed is a low-pass filtered version of the torque and the inertia of the system is relatively high, the speed drops with no visible oscillations (Fig. 5a, left plot).

It is worth noting that the results obtained with strategy P1 confirm a correct post-fault performance even though the control has not been informed that phases a_1 and c_2 do not contribute anymore to the voltage production. Hence, the erroneous localization of the voltage vectors described in section III.A (see Fig. 3) does not have a critical impact on the post-fault performance. The closed-loop control of the d-q currents can compensate this error as long as the controllers do not have a conflict of interest with the x-y controllers.

Strategy P2 provides the same post-fault performance as P1, hence results with P2 will be omitted for the sake of brevity. In order to verify the capability of P3 to also provide a natural fault tolerance, test 2 is designed to evaluate the influence of the x-y voltage saturation in the post-fault the possibility to further reduce the saturation threshold in order to accelerate the entrance in scenario S1 after the OPF occurrence. The main difference with the medium level saturation is that x-y voltages are reached slightly faster (Fig. 6e, right plot) and this limits to some extent the escalation of the d-q voltage references (Fig. 6d, right plot). Since the action-reaction process is quickly stopped, the d-q current control is not affected and the speed tracking is again fully satisfactory (Fig. 6a, right plot). Reducing the saturation threshold $v_{x'y'}^{max}$ below $5\,V$ may results in the deactivation of the x-y current control in healthy state, eventually converting strategy P3 into P1 (where $v_{x'y'}^{max} = 0$). Conversely, setting the threshold above $5\,V$ slightly diminishes the use of the dc-link voltage because it is necessary to produce higher values of x'-y' voltages (see Fig. 5e). The general procedure to set the saturation limit is to experimentally explore the whole operating range in order to guarantee that the threshold is high enough to avoid the saturation in healthy operation.

Test 3 explores the dynamic performance of strategy P3 after the OPF. In the results shown in Fig. 7 the machine is operated with OPF in a_1 and c_2 when the speed reference is changed from 300 rpm to 500 rpm at no load with a d-current reference of 1.1 A. The low value of the x-y saturation threshold ($5\,V$) maintains the x-y current control in open-loop mode and the d-q current control is done in a similar manner as in pre-fault condition. The d-current is maintained around the reference value, showing a good decoupling performance (Fig. 7b). The q-current is increased during the acceleration (at $t = 10s$) and decreased when the machine reaches the new steady-state condition at 500 rpm. The d-q voltages are provided by the d-q current controllers (Fig. 7d) and the x'-y' currents change during the transient according to restrictions from (4). The final speed performance of FOC. For this purpose, three different levels of x'-y' voltage saturation threshold have been defined: high saturation level $v_{x'y'}^{max} = 110\,V$, medium saturation level $v_{x'y'}^{max} = 25\,V$ and low saturation level $v_{x'y'}^{max} = 5\,V$ (left, middle and right plots in Fig. 6, respectively). The x-y PI parameters are those with high gains in table II for all results compared in Fig. 6.

The results shown in the left plots of Figs. 5 and 6 are the same, hence the previous discussion describing the action reaction process that leads to the speed drop holds here again. Nevertheless, when the x-y saturation threshold is decreased to medium level, the saturation of the x'-y' voltages is reached sooner (Fig. 6e, middle plot). The deactivation of the x-y closed-loop control is sufficiently fast to stop the action-reaction process and thus keep the q-voltage unsaturated (Fig. 6d, middle plot). Scenario S1 is automatically entered in this case and the q-current control remains active (Fig. 6b, middle plot). Maintaining the d-q current control active allows the drive to perform the torque control that keeps the machine speed around its target value (Fig. 6a, middle plot).

Comparing the speed and currents of strategy P1 (Fig. 5, right plots) and strategy P3 (Fig. 6, middle plots) it can be observed that the performance is mostly similar among them and also similar to the results that have been reported when the control strategy is reconfigured after the OPF occurrence [11]. It is then confirmed that strategy P3 has the same passive fault tolerance than P1, but it maintains the pre-fault x-y closed-loop control. Right plots in Fig. 6 finally explore tracking is satisfactory during the transient (Fig. 7a). All in all, the transient performance of the drive in post-fault condition is mostly similar to the one in pre-fault condition (and also similar to the performance that is obtained when the control is reconfigured) because the dynamics in distributed-winding machines are governed by the d-q plane.

Test 4 finally explores the post-fault steady-state performance of the proposed IRFOC when a single OPF occurs in phase a_1 at t=5s (see Fig. 8). If the six-phase machine is regulated using standard FOC with closed-loop x-y current control and high saturation level, the speed tracking is lost after the OPF occurrence (Fig. 8a, left plot). The speed drops as in test 1, and the reason is again that the conflict of α-β and x-y controllers eventually ends up in scenario S2, hence losing the torque control. However, in this case the ripple of the d-q currents and torque (Figs. 8b and 8d, left plots) is much higher because the OPF does not have the symmetry shown in test 1 (where phases a_1 and c_2 were spatially shifted by 90°). The higher distortion of the torque leads in this case to visible speed oscillations in post-fault situation, this being similar as in the reconfigured fault-tolerant control. On the contrary, the proposed FOC with natural fault tolerance (Fig. 8, right plots) succeeds to maintain the speed because the x-y current control is performed in open-loop mode after the OPF, and therefore the conflict of controllers is no longer present. The restriction of the fault ($i_x = -i_\alpha$) can be observed in Fig. 8c, right plot, whereas the ripple of the d-q currents and torque is highly reduced (Figs. 8b and 8d, right plots) compared to the case with conventional FOC. Since the conflict of controllers has been skipped and the torque ripple is kept within acceptable limits, the speed is properly tracked with no visible oscillations (Fig. 8a, right plot). This test complements the results of test 1 and confirms that the

satisfactory post-fault performance does not depend on the fault scenario.

As a main conclusion of tests 1 to 4, it can be stated that the natural fault-tolerant capability of the proposed IRFOC can be extended to any fault scenario if the conflict between α-β and x-y controllers is avoided. While the resulting performance is maintained as in reconfigured fault-tolerant control, the natural approach provides further simplicity and immunity against fault detection delays or errors.

V. Conclusion

Most of the research works on multiphase drives achieve the fault-tolerant capability with a mandatory reconfiguration of the control scheme. However, this paper approaches the problem from a different perspective, firstly understanding why pre-fault FOC schemes misbehave under OPF and then suggesting the manner to achieve a natural fault tolerance.

The two main causes of error after the OPF are *i)* the erroneous localization of the applicable voltage vectors and *ii)* the conflict of interest of d-q and x-y controllers. While cause *i)* can be compensated by the closed-loop nature of the d-q current control, the action-reaction process from *ii)* leads to an unstable voltage reference escalation that eventually deactivates the torque/speed control.

Since *ii)* is the main cause of disturbance, keeping the x-y control in open-loop mode allows a natural post-fault operation. This can be achieved with three different approaches: using an open-loop x-y current control in healthy and faulty situation (strategy P1), switching from closed-loop to open-loop mode after the fault occurrence (strategy P2) or setting a low threshold for the x-y voltage saturation level (strategy P3). Even though the three approaches prove to be valid, only P3 ensures a natural fault tolerance with an efficient pre-fault control.

The analysis provided in this work shows that it is possible to naturally achieve a fault-tolerant capability with simple actions that avoid the need to reconfigure the control software. In this regard, the use of the natural approach presents two significant advantages compared to the reconfigured FOC: *i)* Simplicity: because there is no need to modify the control scheme after the OPF occurrence, and *ii)* Robustness: since the drive control becomes immune to fault detection delays or errors. Future directions for research include the design of fault detection methods without localization to be used together with natural fault-tolerant FOC strategies.

References

[1] E. Levi, F. Barrero and M.J. Duran, "Multiphase machines and drives – Revisited," *IEEE Trans. on Ind. Electron.*, vol 63, no. 1, pp. 429-432, 2016.

[2] M.J. Duran and F. Barrero, "Recent Advances in the design modelling, and control of multiphase machines – Part II", *IEEE Trans. on Ind. Electron.*, vol. 63, no. 1, pp. 459-468, 2016.

[3] V. Yaamasu, A. Dekka, M.J. Duran, S. Kouro and B. Wu, "Permanent magnet synchronous generator-based wind energy conversion systems: survey on power converters and controls," *IET Electric Power Appl.*, vol. 11, no. 6, 2017.

[4] M.J. Duran, E. Levi and F. Barrero, "Multiphase electric drives, introduction", *Wiley EEEE*. pp. 1–26, 2017.

[5] E. Levi, R. Bojoi, F. Profumo, H.A. Toliyat and S. Williamson "Multiphase induction motor drives - a technology status review," *IET Electric Power Appl.*, vol. 1, no. 4, pp 489-516, 2007.

[6] A. S. Abdel-Khalik, A. Massoud and S. Ahmed, "Nine-phase six-terminal pole-amplitude modulated induction motor for electric vehicle applications," *IET Electric Power Applications*, DOI. 10.1049/iet-epa.2018.5796, 2019.

[7] M. Tousizadeh, H.S. Che, N.A. Rahim, J. Selvaraj and B.T. Ooi, "Performance Comparison of Fault-Tolerant Three-Phase Induction Motor Drives Considering Current and Voltage Limits," *IEEE Trans. on Ind. Electron.*, Early Access, 2018

[8] J-S. Wang and G-H. Yang, "Data-Driven Output-Feedback Fault-Tolerant Compensation Control for Digital PID Control Systems With Unknown Dynamics," *IEEE Trans. on Ind. Electron.*, vol. 63, no. 11, pp. 7029-7039, 2016 .

[9] H.S. Che, M.J. Duran, E. Levi, M. Jones, W.P. Hew and N.A. Rahim, "Post-fault operation of an asymmetrical six-phase induction machine with single and two isolated neutral points," *IEEE Trans. on Power Electron.*, vol. 29, no. 10, pp. 5406-5416, 2014

[10] I. Gonzalez-Prieto, M.J. Duran, F. Barrero, M. Bermudez and H. Guzman, "Impact of post-fault flux adaptation on six-phase induction motor drives with parallel converters," *IEEE Trans. on Power Electron.*, vol 32, no. 1, pp. 515-528, 2017.

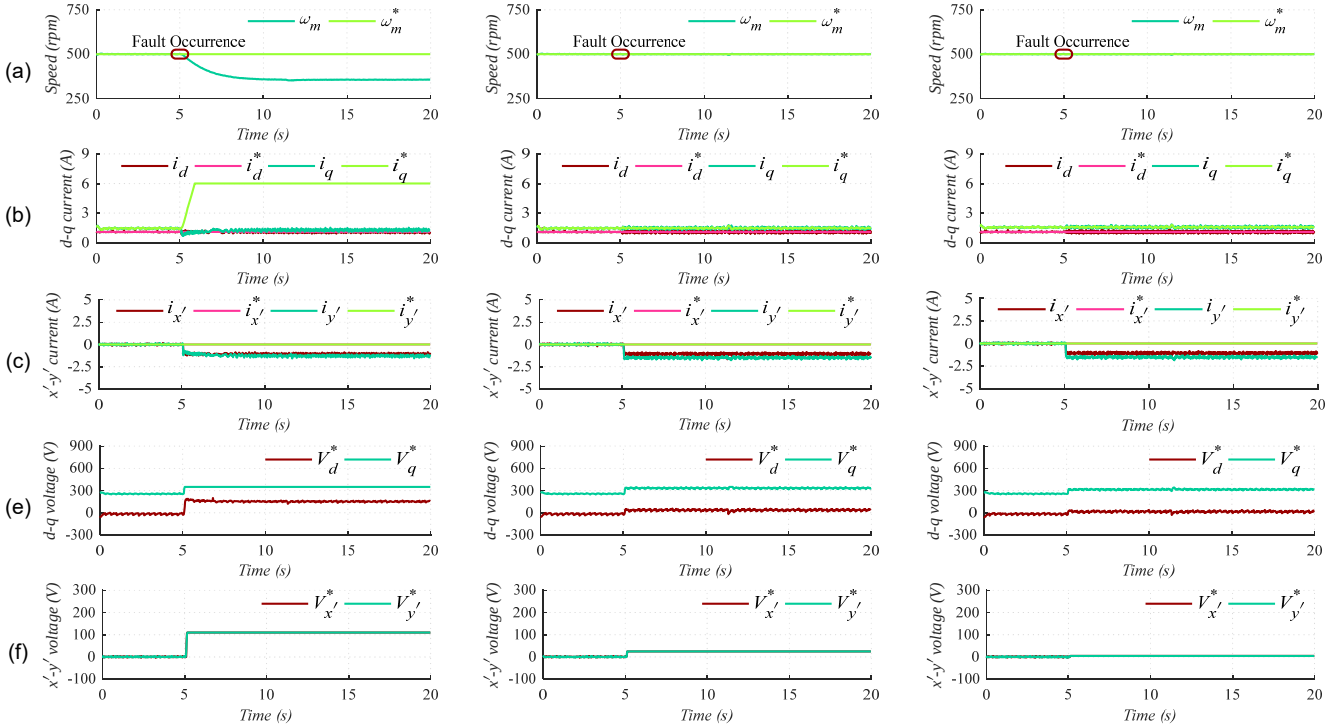

Fig. 6. Transition from pre- to post-fault situations for IRFOC with high saturation level $v_{xyy\prime}^{max} = 110\ V$ (left column), medium saturation level $v_{xyy\prime}^{max} = 25\ V$ (middle column) and low saturation level $v_{xyy\prime}^{max} = 5\ V$ (right column). From top to bottom: (a) Motor speed, (b) d-q currents, (c) x'-y' currents, (d) d-q voltages and (e) x'-y' voltages.

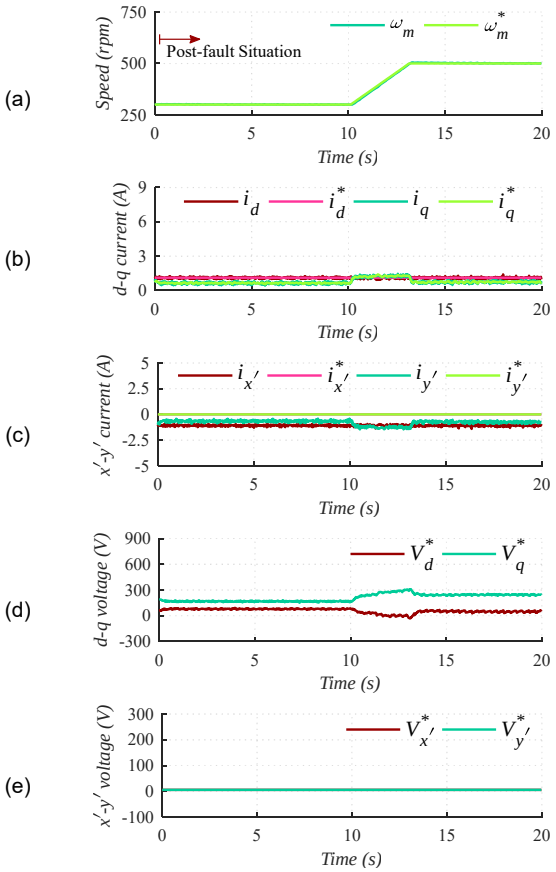

Fig. 7. Speed ramp test for IRFOC with low saturation level $v_{x'y'}^{max} = 5\,V$ (right column). From top to bottom: (a) Motor speed, (b) d-q currents, (c) x'-y' currents, (d) d-q voltages and (e) x'-y' voltages.

[11] W. N. W. A. Munim, M. J. Duran, H. S. Che, M. Bermudez, I. González.-Prieto and N. A. Rahim, "A unified analysis of the fault tolerance capability in six-phase induction motor drives," *IEEE Trans.on Power Electron.*, vol. 32, no. 10, pp. 7824-7836, 2017.

[12] I. Gonzalez-Prieto, M.J. Duran and F. Barrero, "Fault-tolerant control of six-phase induction motor drives with variable current injection," *IEEE Trans. on Power Electron.*, vol. 32, no. 10, pp. 7894-7903, 2017

[13] F. Baneira, J. Doval-Gandoy, A. G. Yepes, Ó. López and D. Pérez-Estévez, "Control strategy for multiphase drives with minimum losses in the full torque operation range under single open-phase fault," *IEEE Trans.on Power Electron.*, vol. 32, no. 8, pp. 6275-6285, 2017.

[14] F. Baneira, J. Doval-Gandoy, A. G. Yepes, Ó. López and D. Pérez-Estévez, "Comparison of post-fault strategies for current reference generation for dual three-phase machines in terms of converter losses," *IEEE Trans. on Power Electron.*, vol. 32, no. 11, pp. 8243-8246, 2017.

[15] M.J. Duran, I. Gonzalez-Prieto, N. Rios-Garcia and F. Barrero, "A simple, fast and robust open-phase fault detection technique for six-phase induction motor drives," *IEEE Trans. on Power Electron.*, vol. 33, no. 1, pp. 547-557, 2018.

[16] I. González-Prieto, M.J. Duran, N. Rios-Garcia, F. Barrero and C. Martín, "Open-switch fault detection in five-phase induction motor drives using model predictive control," *IEEE Trans.on Ind. Electron.*, vol. 65, no. 4, pp. 3045-3055, 2018.

[17] M. Bermudez, I. Gonzalez-Prieto, F. Barrero, H. Guzman, X. Kestelyn and M.J.Duran, "An experimental assessment of open-phase fault-tolerant virtual-vector-based direct torque control in five-phase induction motor drives," *IEEE Trans. on Power Electron.*, vol 33, no. 3, pp. 2774-2784, 2017.

[18] H. Guzman, M.J. Duran, F. Barrero, L. Zarri, B. Bogado, I. Gonzalez-Prieto and M.R. Arahal, "Comparative study of predictive and resonant controllers in fault-tolerant five-phase induction motor drives," *IEEE Trans. on Ind. Electron.*, vol. 63, no. 1, pp. 606-617, 2016.

[19] M.J. Duran, I. Gonzalez-Prieto, M. Bermudez, F. Barrero, H. Guzman and M.R. Arahal, "Optimal fault-tolerant control of six-phase induction motor drives with parallel converters," *IEEE Trans.on Ind. Electron.*, vol. 63, no. 1, pp. 629-640, 2016.

[20] A. S. Abdel-Khalik, M. S. Hamad, A. M. Massoud and S. Ahmed, "Postfault operation of a nine-phase six-terminal induction machine under single open-line fault," *IEEE Trans. on Ind. Electron.*, vol. 65, no. 2, pp. 1084-1096, 2018.

[21] N. Bianchi, S. Bolognani and M. Dai Pre, "Strategies for the fault-tolerant current control of a five-phase permanent-magnet motor," *IEEE Trans. on Ind. Appl.*, vol. 43, no. 4, pp. 960-970, 2007.

[22] E. Levi. In The Industrial Electronics Handbook: Power Electronics and Motor Drives, 2nd ed. Willamowski, B. M.; and Irwin, JD., Eds.; CRC Press:Taylorand FrancisGroup:Boca Raton, FL, pp 3.1–3.31 and 24.1–24.32, 2011.

[23] R. Bojoi, M. Lazzari, F. Profumo and A. Tenconi "Digital field-oriented control for dual three-phase induction motor drives," *IEEE Trans. on Ind. Appl.*, vol. 39, no. 3, pp. 752-760, 2003.

[24] R. Bojoi, F. Farina, M. Lazzari, F. Profumo, A. Tenconi, "Analysis of the asymmetrical operation of dual three-phase induction machines", *in Proc. IEEE Int. Conf, Electric Machines and Drives. (IEMDC'03)*, vol. 1, pp. 429-435, 2003.

[25] H.S. Che, E. Levi, M. Jones, W.P. Hew and N.A. Rahim, "Current control methods for an asymmetrical six-phase induction motor drive," *IEEE Trans. on Power Electron.*, vol 29, no. 1, pp. 407-417, 2014.

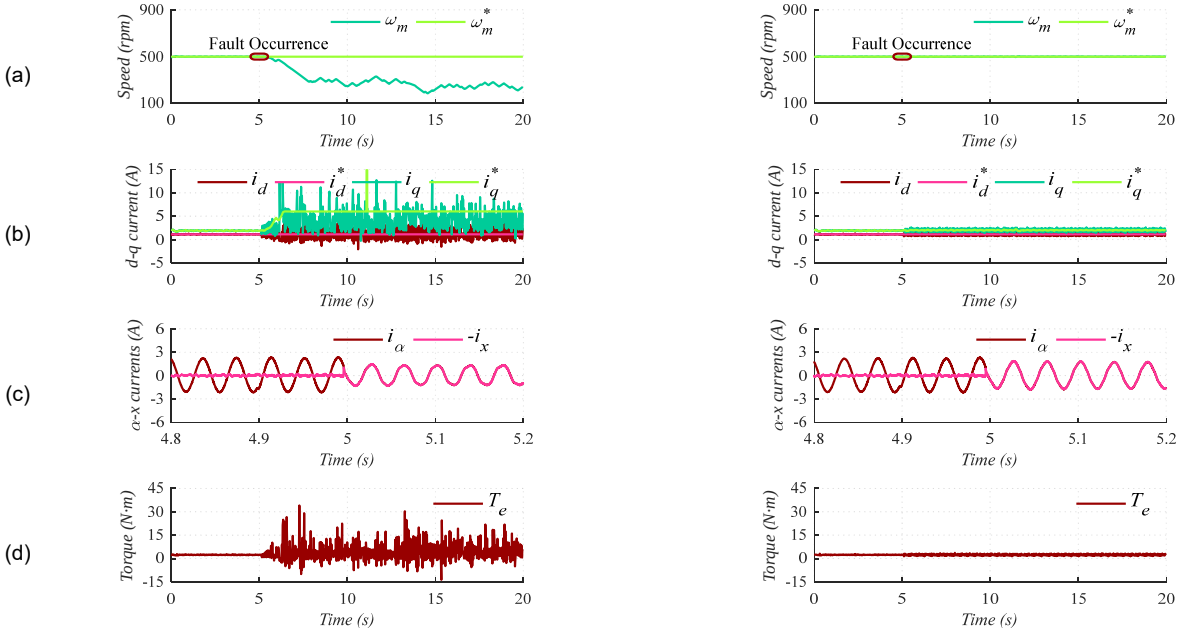

Fig. 8. Transition during a single OPF for IRFOC with high saturation level $v_{x'y'}^{max} = 110\,V$ (left column) and low saturation level $v_{x'y'}^{max} = 5\,V$ (right column). From top to bottom: (a) Motor speed, (b) d-q currents, (c) α-x currents and (d) electromagnetic torque.

[26] R. Kianinezhad, B. Nahid, F. Betin and G.A. Capolino, “A new field orientation control of dual three phase induction machines,” *IEEE Iternaational Conference on Industrial Technology (IEEE ICIT’04).* DOI. 10.1109/ICIT.2004.1490280.

[27] I. Gonzalez-Prieto, M.J. Duran, J.J. Aciego, C. Martin and F. Barrero, “Model predictive control of six-phase induction motor drives using virtual voltage vectors,” *IEEE Trans. on Ind. Electron.*, vol. 65, no. 1, pp. 27-37, 2018.

[28] E. Levi, “Advances in converter control and innovative exploitation of additional degrees of freedom for multiphase machines,” *IEEE Trans. on Ind. Electron*., vol 63, no. 1, pp. 433-448, 2016.

[29] A. Yepes, J.A. Riveros, J. Doval-Gandoy, F. Barrero, O. Lopez, B. Bogado, M. Jones and E. Levi, “Parameter identification of multiphase induction machines with distributed windings-part 1: sinusoidal excitation methods,” *IEEE Trans. on Energy Conv.*, vol. 27, no. 4, pp. 1056-1066, 2012.

[30] J.A. Riveros, A. Yepes, F. Barrero, J. Doval-Gandoy, B. Bogado, O. Lopez, M. Jones and E. Levi, “Parameter identification of multiphase induction machines with distributed windings-part 2: time-domain techniques,” *IEEE Trans. on Energy Conv.*, vol. 27, no. 4, pp. 1067-1077, 2012.

[31] S. Khadraoui, M.A. Fnaiech, H.N. Nounou, M.N. Nounou, J. Guzinski, H. Abu-Rub, A. Datta & S.P. Bhattacharyya “Measurement-based control approach for tuning PID controllers: application to induction machines,” *Journal of Control and Decision*, vol. 3, no. 3, pp. 179-196. 2016.

Ignacio González Prieto was born in Malaga, Spain, in 1987. He received the Industrial Engineer and M.Sc. degrees in fluid mechanics from the University of Malaga, Malaga, Spain, in 2012 and 2013, ´ respectively, and the Ph.D. degree in electronic engineering from the University of Seville, Sevilla, Spain, in 2016. His research interests include multiphase machines, wind energy systems, and electrical vehicles

Mario J. Duran was born in Bilbao, Spain, in 1975. He received the M.Sc. and Ph.D. degrees in electrical engineering from the University of Malaga, Malaga, in 1999 and 2003, respectively. He is currently a Full Professor in the Department of Electrical Engineering, University of Malaga. His research interests include modeling and ´ control of multiphase drives and renewable energies conversion systems.

Paula Garcia-Entrambasaguas was born in Málaga, Spain, in 1992. She received the University and Master’s degrees in Industrial Engineering from the University of Málaga, in 2015 and 2017, respectively.
She is currently working toward the Ph.D. degree in the Electric Power Systems program at University of Málaga, Spain. Her research focuses on multiphase machines and drives and on control methods in pre- and post-fault situations.

Mario Bermudez was born in Málaga, Spain, in 1987. He received the B.Eng. degree in industrial engineering from the University of Málaga, Málaga, Spain, in 2014, and the Ph.D. degree in electrical/electronic engineering jointly from Arts et Métiers ParisTech, Lille, France, and from the University of Seville, Seville, Spain, in 2018. He is currently a Substitute Professor in the Department of Electrical Engineering, University of Huelva, Huelva, Spain. His research interests include modeling and control of multiphase drives, digital signal processor-based systems, and electrical vehicles.